4166 *Chem. Mater.* **2010,** *22,* 4166–4174
DOI:10.1021/cm100614e

CHEMISTRY OF MATERIALS
Article

Dewetting-Induced Formation of Periodic Dot Arrays of Polymer/Au Composites by Capillary Force Lithography

Minwoo Park,[†] Dong Choon Hyun,[†] Joohee Kim,[‡] Youn Sang Kim,*[,‡] and Unyong Jeong*[,†]

[†]*Department of Materials Science and Engineering, Yonsei University, 134 Shinchon-dong, Seoul, Korea, and* [‡]*Department of Nano Science and Technology, Graduate School of Convergence Science and Technology, Seoul National University, 864-1, Iui-dong, Yeongtong-gu, Suwon-si, Gyeonggi-do, Korea*

Received February 27, 2010. Revised Manuscript Received May 18, 2010

This paper demonstrates that simple cross-stamping in capillary force lithography (CFL) enables the fabrication of periodic dots, rings, and line patterns of the metal/polymer composites. The key to the success was the compatibility of polymer/inorganic precursor composite liquids on substrates. As a model study, the composites consisting of poly(ethylene oxide) (PEO) and the gold precursor ($HAuCl_4$) were investigated. The contact angle of the composite liquid on the Si substrate significantly increased when the fractional composition of the precursor was over a critical value, while the contact angle on poly(dimethylsiloxane) (PDMS) molds decreased. The reduced wettability on the substrate resulted in isolated dot patterns upon cross-stamping on the line patterns fabricated by CFL. The shape, size, and number of the dots could be controlled by adjusting the thickness of the composite films. Small coupled dots were obtained from dual-line patterns and large single dots were obtained from single-line patterns. When the initial film thickness was ~60 nm, the cross-stamping resulted in donutlike composite patterns. Chemical reduction of the precursor could generate periodic arrays of Au rings or solid nanodots.

1. Introduction

In recent years, various advanced unconventional lithography has been developed, including nanoimprint lithography,[1−3] soft lithography,[4−6] capillary force lithography (CFL),[7] and soft molding.[8] Such techniques allow the patterning and transferring micrometer- and nanometer-scale features without having to utilize complicated and expensive optical apparatus. Among those unconventional lithographic methods, CFL has been gaining strong interest, because of the simple process and the reliable fidelity of pattern transfer.[9] In CFL, a variety of complex patterns can be created by controlling the annealing temperature and the thickness of polymeric layers on substrates. Double stamping with an additional stamp can diversify the patterns accessible via CFL even more.[10,11] It has been reported that appropriate tuning of the process conditions and material properties such as surface energy and viscosity can lead to a dramatic reduction in the residual layers.[12] Since various functional polymeric materials can be directly patterned on the nanometer scale with CFL, desired patterns can be obtained without sequential etching or deposition process.[13,14]

The use of polymer/inorganic composites as the layers patterned by CFL may enable the high throughput and high-speed formation of periodically arrayed inorganic nanomaterials. Typical processes to obtain the final inorganic nanopatterns start with the pattern formation of polymer/inorganic precursor composites, followed by chemical reduction to produce pure inorganic materials. However, there have been no systematic studies about the effect of the inorganic precursors on the morphology which will determine the pattern of the target inorganic materials. In this paper, we demonstrated that the surface energy of the polymer/precursor composite films can change, to a significant degree, as the fractional composition of the precursor increases. The surface energy change led to completely different patterns by CFL. The decreased wettability of the composite layer to the substrate and the increased compatibility to the wall of the stamp

*Authors to whom correspondence should be addressed. E-mails: younskim@snu.ac.kr (Y.S.K.), ujeong@yonsei.ac.kr (U.J.).

(1) Chou, S. Y.; Krauss, P. R.; Renstrom, P. J. *J. Vac. Sci. Technol.* **1996**, *14*, 4129.
(2) Guo, L. J. *Adv. Mater.* **2007**, *19*, 495.
(3) Chou, S. Y.; Krauss, P. R.; Renstrom, P. J. *Science* **1996**, *272*, 85.
(4) Xia, Y.; Whitesides, G. M. *Angew. Chem., Int. Ed.* **1998**, *37*, 550.
(5) Truong, T. T.; Lin, R.; Jeon., S.; Lee, H. H.; Maria, J.; Gaur, A.; Hua, F.; Meinel, I.; Rogers, J. A. *Langmuir* **2007**, *23*, 2898.
(6) Odom, T. W.; Love, C.; Wolfe, D. B.; Paul, K. E.; Whitesides, G. M. *Langmuir* **2002**, *18*, 5314.
(7) Suh, K. Y.; Kim, S. Y.; Lee, H. H. *Adv. Mater.* **2001**, *13*, 1386.
(8) Kim, Y. S.; Suh, K. Y.; Lee, H. H. *Appl. Phys. Lett.* **2001**, *79*, 2285.
(9) Bruinink, C. M.; Péter, M.; Maury, P. A.; de Boer, M.; Kuipers, L.; Huskens, J.; Reinhoudt, D. N. *Adv. Funct. Mater.* **2006**, *16*, 1555.
(10) Jung, J.-M.; Stellacci, F.; Jung, H.-T. *Adv. Mater.* **2007**, *19*, 4392.
(11) Suh, K. Y.; Lee, H. H. *Adv. Funct. Mater.* **2002**, *12*, 405.
(12) Kim, Y. S.; Lee, H. H. *Adv. Mater.* **2003**, *15*, 332.
(13) Duan, X.; Zhao, Y.; Perl, A.; Berenschot, E.; Reinhoudt, D. N.; Huskens, J. *Adv. Funct. Mater.* **2010**, *20*, 663.
(14) Jeong, H. E.; Lee, S. H.; Kim, P.; Suh, K. Y. *Nano Lett.* **2006**, *6*, 1508.

 Published on Web 07/01/2010

allowed the fabrication of isolated dot patterns by simply cross-stamping the premade line patterns. As a model study, we focused on the composite of poly(ethylene oxide) (PEO) and the gold precursor ($HAuCl_4$), since the periodic array of Au nanoparticles is immediately applicable to the sensors based on localized surface plasmon resonance.[15,16] This study demonstrated the formation of solid dots and rings of Au obtained by controlling the surface energy and thickness of the composite films. The process described in this report can be easily extended to large-area patterning of nanometer-sized Au features with high throughput, which is immediately applicable to biosensors.

2. Experimental Sections

Materials. Poly(ethylene oxide) (PEO, M_w = 100 000), gold-(III) chloride trihydrate (99.9+%), hydrazine hydrate (N_2H_4, reagent-grade, 50%−60%), and 2,2,2-trifluoroethanol (TFE, ≥99%) were purchased from Sigma−Aldrich. The Sylgard 184 elastomer kit used to make the PDMS stamps was purchased from Dow Corning. Trichloroethylene (TCE, 99.5%) was purchased from DC Chemical Co., Ltd.

Fabrication of Composite Single-Line Patterns or Dual-Line Patterns. The poly(dimethylsiloxane) (PDMS) prepolymer and cross-linker were mixed at 5:1 (w/w) and poured in line-and-space PET masters, and then cured at 55 °C for 24 h. The dimensions of the as-prepared PDMS stamps were line/space = 1 μm/2.2 μm and 1.2 μm/1.5 μm (see Figure S1 in the Supporting Information). Silicon wafers were cleaned ultrasonically with TCE, acetone, and methanol for 5 min, followed by rinsing with deionized (DI) water and drying with nitrogen gas. PEO and $HAuCl_4$ were dissolved in TFE with varying atomic ratio α (α = [$HAuCl_4$]/[EO]). The 70-nm-thick and 20-nm-thick films were prepared by spin-coating the PEO solution with 0.6 and 0.3 wt % in TFE, respectively. The spin coating was performed on silicon wafers at 3000 rpm for 30 s. For 60-nm-thick films, the concentration of the PEO solution was the same as the 70-nm-thick films but spin-coated at 3500 rpm for 30 s. The PDMS stamps (line/space = 1 μm/2.2 μm) were conformal, contacted on the polymer composite thin films, and then annealed at 80 °C under vacuum. After 10 min, the samples were cooled at room temperature in air and lifted slowly from the silicon wafer. Afterward, the PDMS stamp (line/space = 1.2 μm/1.5 μm) were cross-contacted on the composite line patterns. The thermal annealing and removal of the PDMS patterns was the same.

Contact-Angle Measurement of the Composite Films on the PDMS Stamp and Silicon Substrate. The PDMS prepolymer mixed with the cross-linker (5:1, w/w) was spin-coated on a silicon wafer at 4000 rpm for 60 s and cured at 55 °C for 1 day. Dilute polymer/$HAuCl_4$ solution with different atomic ratio (α = [$HAuCl_4$]/[EO]) in TFE was spin-coated on the PDMS layer. All the samples were annealed at 80 °C for 3 min to make the composite dewet on the substrate. The height and width of the dewetted composite films were analyzed by atomic force microscopy (AFM). The AFM images are shown in Figure S2 in the Supporting Information. We assumed that these profiles of the drops were partially spherical. We measured the radius using the Pythagorean Theorem to obtain the contact angles (θ). This assumption can describe the shape of the droplets very well with small deviation from the true contact angles and it can remove some vagueness in contact angle measurement.[17,18] The average value of contact angles was obtained from 10 drops for each sample.

Formation of Au Dots and Rings. The specimens were stuck to the bottom of the cap of a conical tube (50 mL). Hydrazine hydrate (0.01 mL) was dropped in the conical tube and sealed tightly. Within 3 min, reduction of $HAuCl_4$ to Au particles was completed. Au rings were obtained by simply annealing the reduced sample at 350 °C for 20 min in air. Instead of Au rings, solid Au dots were generated by first flipping over the specimens and annealed them at 130 °C. Further calcinations at 350 °C in air for 20 min produced solid Au dots.

Analysis. The thickness of $HAuCl_4$/PEO composite films was measured by an ellipsometer (SE MG-1000, Nanoview Co.). The topologies of the composite line patterns were examined by optical microscopy (OM) (Model BX 51, Olympus Co.), atomic force microscopy (AFM) (Model Dimension 3100, Digital Instrument Co.), and field-emission scanning electron microscopy (FE-SEM) (Model S-4300, Hitachi Co.). Contact angles of the composite films on PDMS and morphologies for the Au/PEO and the pure Au dot patterns were analyzed by AFM. A Fourier transform infrared spectroscopy (FT-IR) (Model TENSOR 37, Bruker Co.) study was performed to investigate the degree of the coordination with varying molar ratio (α) of $HAuCl_4$, the polymer/$HAuCl_4$ mixture solution was spin-coated on KBr substrates and then annealed at 80 °C. The FT-IR study was conducted in a transparent mode.

3. Results and Discussions

The kinetics by the CFL is strongly dependent on the viscosity of liquids.[12] Glassy amorphous polymers such as polystyrene (PS) possess high viscosities at the regular processing temperatures of CFL. The significant extension of the long viscoelastic polymer chains along the flow direction in the narrow gap between the stamp and the substrate leads to considerable loss in the chain conformational entropy, which is the main origin of the elastic resistance to the flow of polymeric liquids.[19] The resistance is proportional to their viscosity. Another barrier to the liquid flow is the friction between the extended polymer chains and the rubbery walls of the stamp. The capillary pressure in CFL has been known to be insufficient to completely pull out the polymer chains from the gap; therefore, it leaves a residual layer under the stamp. Contrary to that of amorphous polymers, the viscosity of crystalline polymers dramatically decreases at their melting temperature.[19] The sharp viscosity drop makes it possible for the CFL to proceed without severe increase in the processing temperature. In addition, the high chain mobility helps to remove the residual layer of the polymers. This study employed PEO as a crystalline polymer because PEO has a reasonable melting temperature (~60 °C) and readily forms a complex with organometallic precursors.

Figure 1 exhibits a schematic illustration of the experimental process used in this study. A line-and-space

(15) Haes, A. J.; Van Duyne, R. P. *J. Am. Chem. Soc.* **2002**, *124*, 10596.
(16) Jung, J.-M.; Kwon, K. Y.; Ha, T.-H.; Chung, B. H.; Jung, H.-T. *Small* **2006**, *2*, 1010.
(17) Kim, J. K.; Jeong, W. Y.; Son, J. M.; Jeon., H. K. *Macromolecules* **2000**, *33*, 25.
(18) Kim, J. K.; Jeong, W. Y. *Polymer* **2001**, *42*, 4423.
(19) Ferry, J. D. *Viscoelastic Polymer Fluids* ; Wiley: New York, 1980.

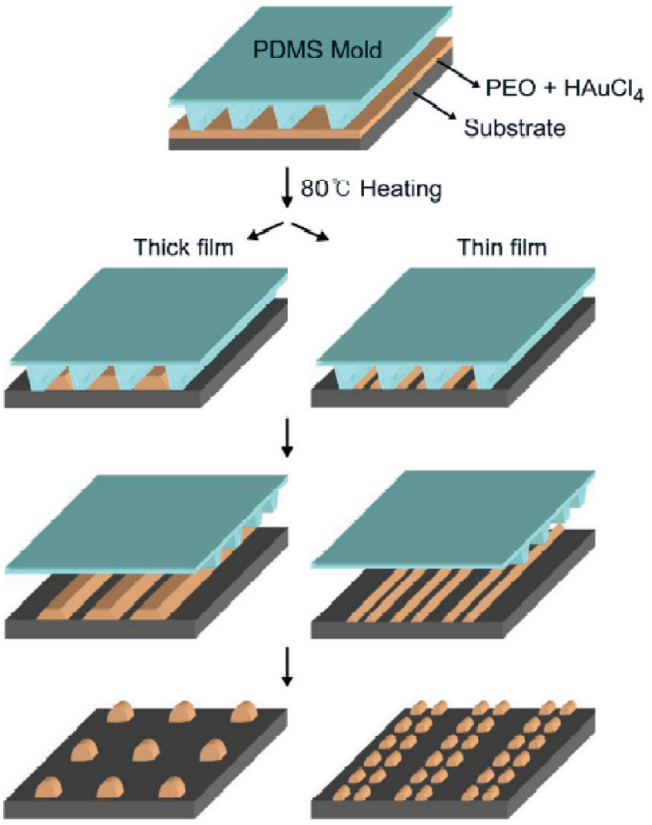

Figure 1. Schematic illustration of the experimental process. Stamping with PDMS stamps on polyethylene oxide (PEO)/$HAuCl_4$ composite films generated isolated single lines or dual lines, depending on the film thickness. Cross-stamping created isolated composite dots.

PDMS stamp was placed on the spin-coated PEO/$HAuCl_4$ composite films, and then thermal heating was applied at 80 °C, which is above the melting temperature of PEO. The capillary force drove the polymer liquid to move toward the empty trenches and generated a single line or dual lines in each PDMS trench. The overall morphology was determined by the volume of the liquid versus the channel width, as well as the contact angle (θ) of the liquid on the PDMS wall and the surface tension of liquid ($\gamma_{polymer/air}$).[7] At equilibrium, the Laplace pressure is equivalent to the gravitational force: that is, $\rho g h_{max} = (2\gamma_{polymer/air} \cos\theta)/L$. Here, ρ is the density and L is the half width of the meniscus. Liquids compatible with the wall of the stamp lead to small contact angles and rise up, to a large extent, on the wall. The half width of the meniscus (L) can be expressed as follows:[7,8]

$$L = \frac{(h_{max} - h_{min})\cos\theta}{1 - \sin\theta} \quad (1)$$

Equation 1 indicates that the meniscus on both side walls may not be connected each other when the volume of the liquid is not sufficient, creating dual lines separated in each trench of the stamp. Meanwhile, the meniscuses meet each other and form a continuous liquid medium when enough volume of the liquid is supplied, forming a single line in each trench. Therefore, the formation of single or dual lines is purely dependent on the thickness of the composite films, as long as the other conditions are fixed. Thermally annealed at 80 °C after the stamp was placed cross on the line pattern, the polymer chains rearranged themselves to minimize the total interfacial energy with the stamp and the substrate. Since the viscosity of the composite film with a very low precursor composition changed to a negligible extent, the morphology of the polymer composites after cross-stamping is determined by the film thickness and the interfacial tensions ($\gamma_{polymer-air}$, $\gamma_{polymer-PDMS}$, $\gamma_{polymer-substrate}$). If the liquid is very compatible to the substrate, it will flow in the stamp trenches and form continuous lines. Meanwhile, if the liquid is so poorly compatible with the substrate that it remains dewetted on the substrate, it may produce isolated dots. Upon cross-stamping on the premade line patterns, single dots will be created from the single-line patterns and coupled dots will be generated from the dual-line patterns, as illustrated in Figure 1. The composite dots can produce an array of isolated Au dots via chemical or thermal reduction.

In the experiment, composite thin films were made by spin-coating a solution of $HAuCl_4$ and PEO in trifluoroethanol (TFE). The good solubility of both $HAuCl_4$ and PEO in TFE prevented phase separation during the spin coating. In addition, the good compatibility of TFE with silicon wafers facilitated conformal coating of the composite films. Figure 2 exhibits the patterns after the first stamping on the composite films with thicknesses of 70 and 20 nm. The atomic ratio of $HAuCl_4$ to ethylene oxide (EO) (denoted as α) was fixed at 0.086. The step height and line width of the line-and-space PDMS stamp were 1 and 2.2 μm, respectively. Figures 2A and 2B are typical line patterns near an air-trapped defect, displayed to prove the formation of single and dual lines in each trench. The defects are generated by dusts on the PDMS substrate. We could not observe such defects with clean PDMS stamps. The traces of the lines from the defect indicate that stamping on the 70-nm-thick film generated a single-line pattern while the same process on the 20-nm-thick film generated a dual-line pattern. Dimensions of the lines were 140 nm in height and 2.2 μm in width for the single-line pattern and 85 nm in height and 800 nm in width for the dual-line pattern (see Figures 2C−F). The profile of the patterned lines showed good uniformity and regularity. The continuous separated line patterns obtained were always the same, regardless of the α value of $HAuCl_4$ in the composite films.

As mentioned previously, the morphology after cross-stamping should be determined by the relative interfacial energies of the liquid with the substrate and the PDMS stamp, as long as the viscosity is low enough, so that the kinetic difference can be neglected. Since the composition of $HAuCl_4$ in this study was very low, compared to the volume of the polymer, we could not observe a viscosity change at 80 °C. Figure 3 exhibits the changes in the contact angles of the composite films on a flat PDMS substrate (Figure 3A) and the silicon wafer (Figure 3B) as the α value of $HAuCl_4$ was increased. The contact angle decreased from $\theta = 76°$ at $\alpha = 0$ to $\theta = 64°$ at $\alpha = 0.02$, and maintained a similar value up to $\alpha = 0.065$. The

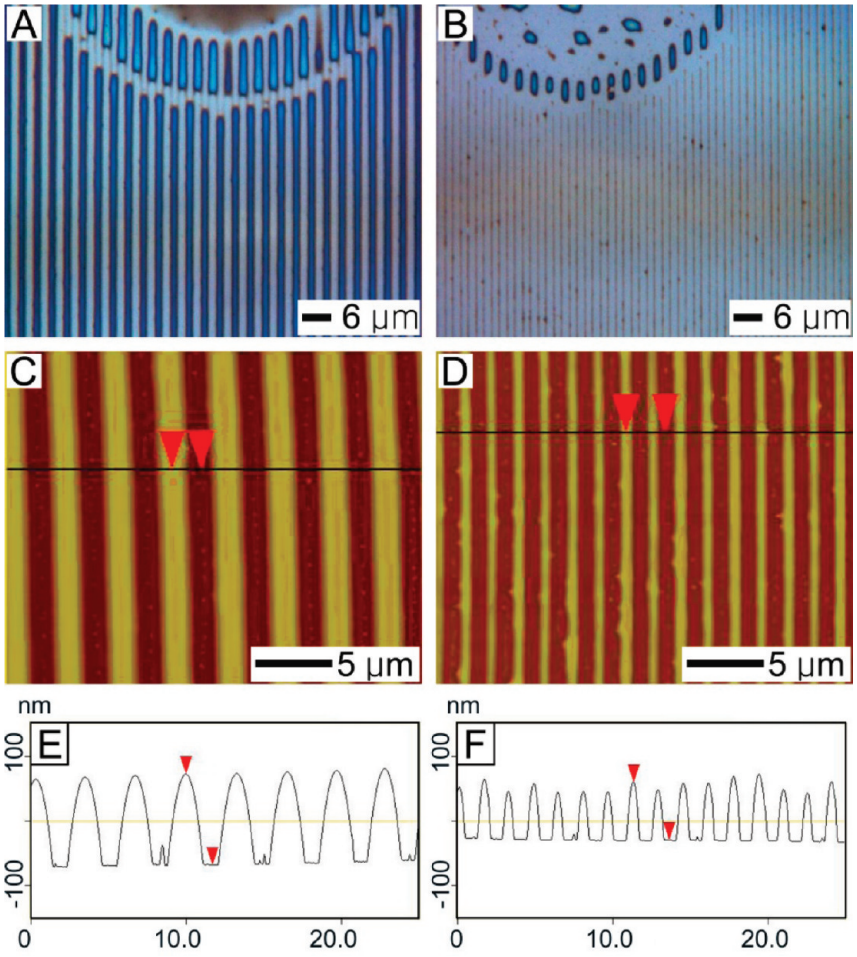

Figure 2. Thickness effect on the line patterns. Optical microscopy images, AFM images, and height profiles of (A, C, E) the single-line pattern obtained from a 70-nm-thick composite film and (B, D, E) the dual-line pattern from a 20-nm-thick composite film. The atomic ratio (α) of $HAuCl_4$ to ethylene oxide ([$HAuCl_4$]/[EO]) was fixed at α = 0.086.

contact angle showed another abrupt decrease at α = 0.075, and then reached values as low as $\theta = 54°$ at α = 0.086. Further increases in the precursor concentration made no changes in θ. At atomic ratios of α > 0.15, phase separation between the precursor and the polymer occurred during spin coating. The contact angle of the polymer composite on the Si wafers increased as α increased. The pure PEO almost completely wetted the surface of the Si wafer. The contact angle reached $\theta = 16°$ at α = 0.065, and then jumped to $\theta = 25°$ at α = 0.086. Again, further increases in the precursor in the composite did not lead to any increase in θ.

The changes in the contact angle must be related with the coordination between $HAuCl_4$ and the protonated oxygen in PEO. We performed FT-IR study to investigate the degree of coordination with varying molar ratio (α) of $HAuCl_4$. The polymer/$HAuCl_4$ mixture solution was spin-coated on KBr substrates and then annealed at 80 °C to make the same condition with the experiments. The FT-IR study was conducted in a transparent mode. The results are exhibited in Figure 4. As shown in the peak profile in Figure 4A, the coordination between $HAuCl_4$ and the oxygen in PEO shifted the C−O−C stretching mode from 1118.68 cm^{-1} for pure PEO to 1105.17 cm^{-1}. Such peak shifts have been reported in previous results.[20] Based on the shift of the peak, the portion of the coordinated oxygen was calculated (Figure 4B). The amount of coordination was proportional to the molar ratio of $HAuCl_4$ and was saturated at α = 0.087, which was highly coincident with the profile of the contact angles, depending on the value of α. This experimental result verifies that the change of contact angles and the saturation resulted from the change of coordination amount and its saturation.

The change in the contact angle led to different wetting behavior on the substrate. Figure 5 exhibits optical images of the single-line patterns of the PEO/$HAuCl_4$ composites after re-annealing at 80 °C for 10 min. The atomic ratio (α) of the precursor was varied: α = 0 (Figure 5A), α = 0.043 (Figure 5B), α = 0.065 (Figure 5C), and α = 0.086 (Figure 5D). When α ≤ 0.043, the polymers spread on the substrate; therefore, the lines become smeared, as shown in Figures 5A and Figure 5B. In contrast, when α ≥ 0.065, the line pattern maintained the initial feature without spreading on the substrate (Figures 5C and 5D). Further annealing at the same temperature did not make any difference. The result

(20) Rabek, J. F.; Lucki, J.; Qu, B. J.; Shi, W. F. *Macromolecules* **1991**, *24*, 836.

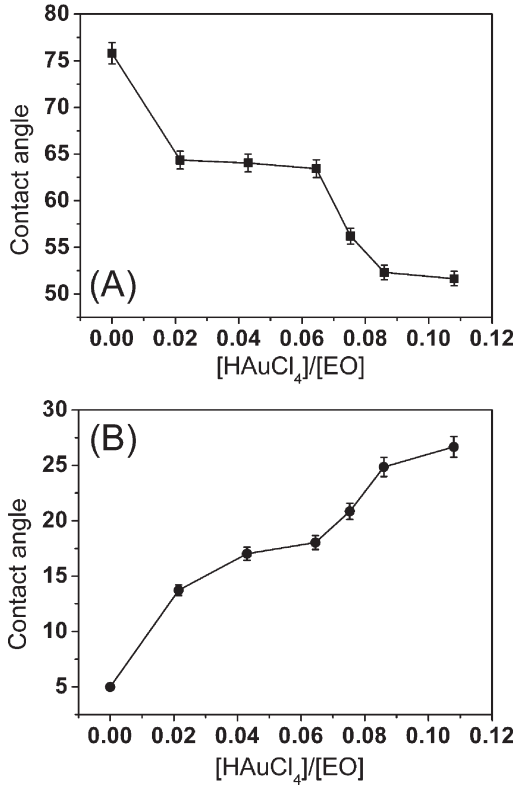

Figure 3. Changes in contact angle of the $HAuCl_4$/PEO composite films on (A) the PDMS and (B) the silicon wafer substrate, according to the atomic ratio of $HAuCl_4$ to ethylene oxide (α). The contact angles sharply changed at α = 0.02 and α = 0.075 on both surfaces.

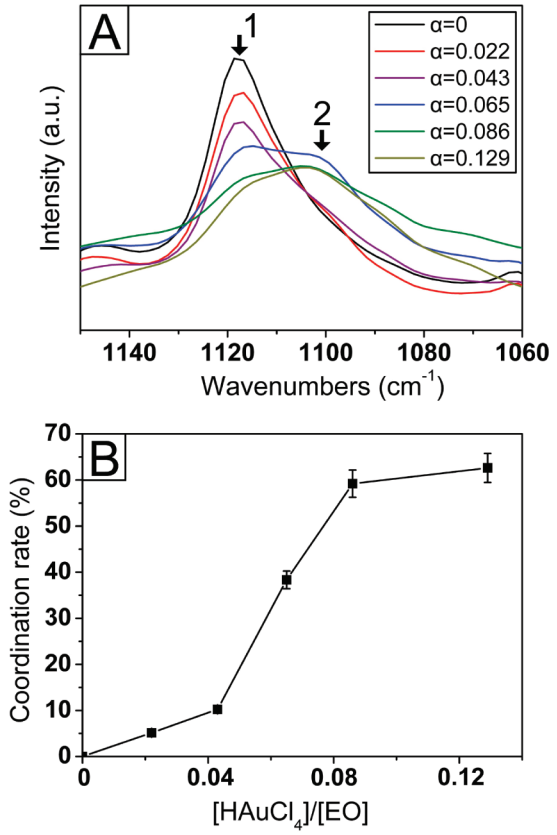

Figure 4. FT-IR study to investigate the degree of coordination between $HAuCl_4$ and the oxygens in PEO: (A) profile change of C−O−C stretching mode, according to the atomic ratio (α) of $HAuCl_4$ to ethylene oxide (the coordination shifted the peak position) and (B) change in the degree of coordination as the value of α increases. In panel A, arrows (1) and (2) indicate the IR C−O−C chains before $AuCl_4^-$ coordination (1118.68 cm^{-1}) and after $AuCl_4^-$ coordination (1105.17 cm^{-1}), respectively.

indicates that a contact angle of $\theta \approx 25°$ is sufficient to keep the composite liquid dewetted on the substrate.

Based on the contact angle changes and the dewetting behavior of the composite films, the morphology after cross-stamping was investigated. Figure 6 shows the self-organization of the composite patterns after cross-stamping with a PDMS stamp (line width of 1.2 μm and a space of 1.5 μm). The thickness of the initial film was fixed at 70 nm that generated single-line patterns. We changed the atomic ratio (α) of $HAuCl_4$: α = 0 (pure PEO) (Figure 6A), α = 0.043 (Figure 6B), and α = 0.086 (Figure 6C). For the pure PEO films or the composite films with a small amount of Au precursor, cross-stamping on the single-line patterns again created the straight single lines in the trenches of the second stamp, as demonstrated in Figures 6A and 6B. Since pure PEO and the composite with a small α value have good affinity to the surface of silicon wafer but are incompatible with the hydrophobic stamp, the liquids spread on the wafer and merged with each other to form a continuous line in each trench. On the other hand, cross-stamping on the composite film with a high precursor composition (α = 0.086) generated the isolated dots, as demonstrated in Figure 6C. The average dimension of each dot was 1.8 μm × 1.1 μm. The maximum height was 170 nm. The formation of the isolated dots is attributed to the decreased compatibility of the liquid to the surface of the wafer, as well as the improved affinity to the walls of the stamp. We found that the minimum atomic ratio of the precursor to generate the isolated dots was 0.086,

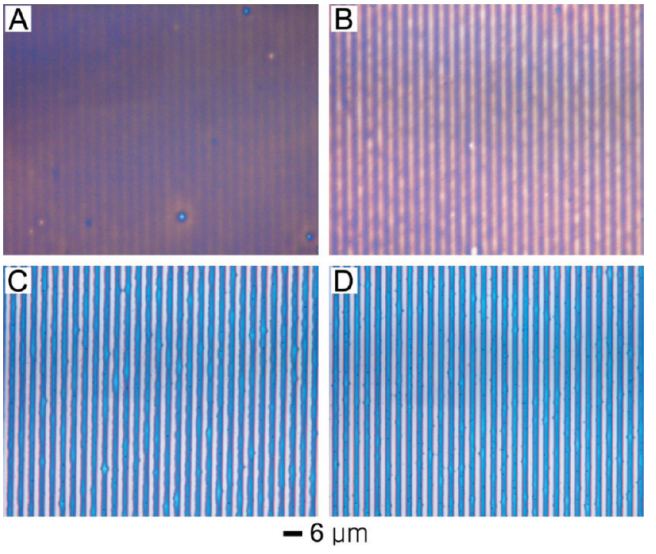

Figure 5. Optical microscopy images obtained after annealing the single-line patterns of PEO/$HAuCl_4$ composites according to the atomic ratio (α) of $HAuCl_4$: (A) α = 0, (B) α = 0.43, (C) α = 0.065, and (D) α = 0.086. The initial thickness of the films was fixed at 70 nm.

which was coincident with the results in contact angle measurement.

We tried to check the residual layer between the dots using an EDX system that was equipped for SEM, but the

resolution did not fit the space between the composite dots. Instead, we used AFM analysis to check it. Figure 7 exhibits the height profiles of the dot patterns after scratching the specimen with a metallic tweezer. The scratched area and the stamped area showed the same height profiles, indicating that there was not a polymeric layer between the dots. Small polymeric debris was found between the dots, but a layer was not detected.

As demonstrated in Figure 2, film thickness is another variable for the morphology by CFL. We fixed the precursor ratio at $\alpha = 0.086$ and varied the thickness. Figure 8 shows the results after cross-stamping on the films with thicknesses of 60 nm (Figure 8A) and 20 nm (Figure 8B). It is noticeable that cross-stamping on the 70-nm-thick films produced solid dots. The 60-nm-thick

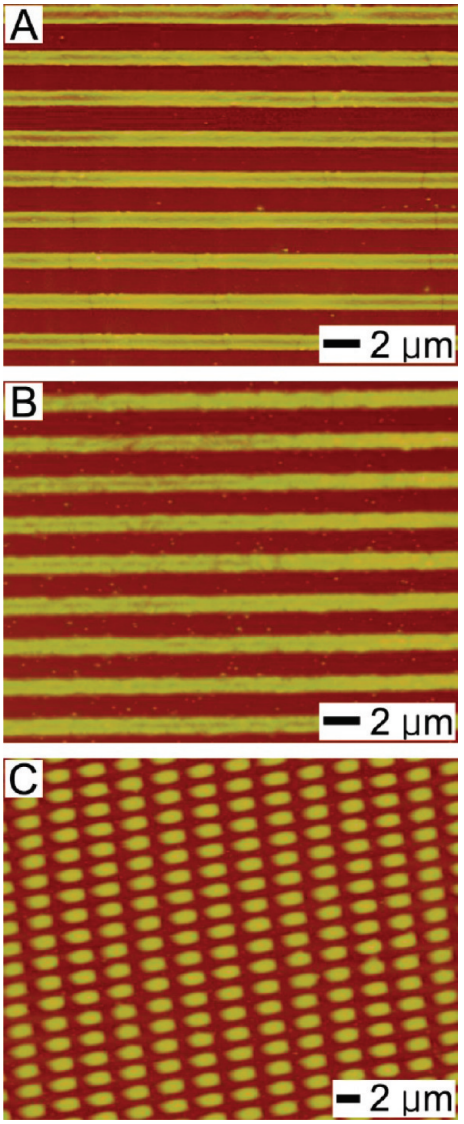

Figure 6. Effect of the atomic ratio (α) of $HAuCl_4$ to ethylene oxide: (A) $\alpha = 0$, (B) $\alpha = 0.043$, and (C) $\alpha = 0.086$. The thickness was fixed at 70 nm.

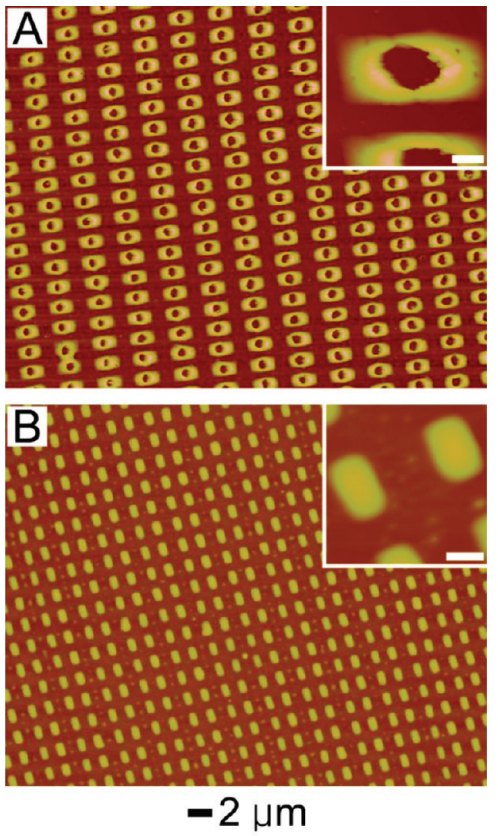

Figure 8. Effect of film thickness during the cross stamping (the atomic ratio (α) of $HAuCl_4$ to ethylene oxide was fixed at $\alpha = 0.086$): (A) hollow dot pattern obtained from a 60-nm-thick film (single-line pattern was formed in the first stamping and cross-stamping generated donutlike dots) and (B) solid dot pattern from a 20-nm-thick film. Dual-line pattern by the first stamping transformed into coupled dots after cross stamping. The scale bar in the inset of each panel is 500 nm.

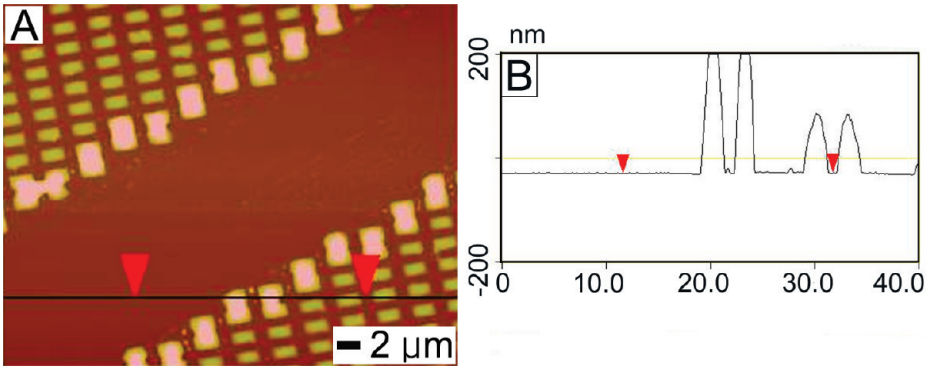

Figure 7. AFM image for checking the existence of a residual polymer layer after cross-stamping the single-line patterns: (a) height image for scratched region of square patterns and (b) height profile between the Si wafer and the PDMS stamped region.

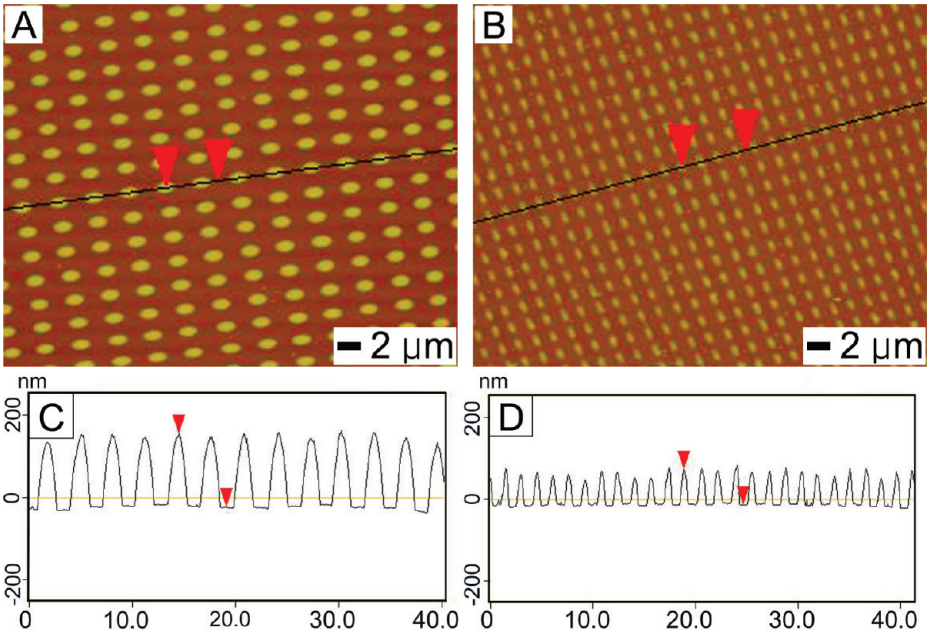

Figure 9. AFM images obtained after flipping over the samples and annealing at 130 °C: (A) AFM image obtained from the single line in Figure 6C and (B) AFM image obtained from the dual line in Figure 8B. (C and D) Height profiles of the AFM images in panels A and B, respectively. The ripening process deleted the remnant small dots around the isolated larger dots.

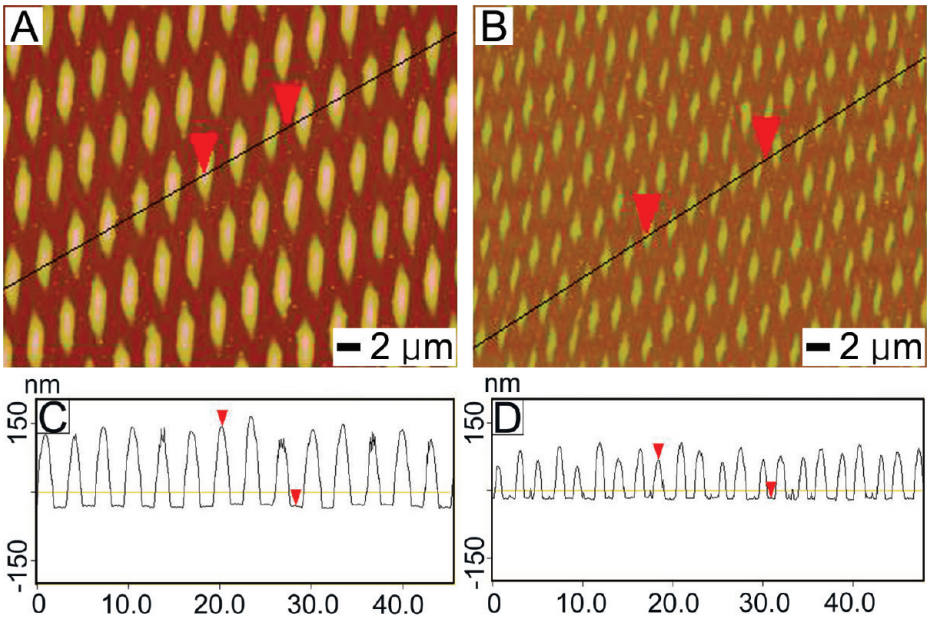

Figure 10. AFM images obtained after 60°-tilted cross-stamping: (A) AFM image obtained from the single line in Figure 2C and (B) AFM image obtained from the dual line in Figure 2D. (C and D) Height profiles of the AFM images in panels A and B, respectively.

film formed a single-line pattern on the first stamping. Cross-stamping produced isolated donut shapes, as seen in Figure 8A. The inset image is an enlargement of one donut shape. AFM investigation reveals that the center of each donut did not contain any residual polymers (see Figure S3 in the Supporting Information). Such dewetting on the substrate originates from the increase in the interfacial energy with the substrate, in addition to the enhanced increase of the liquid on the stamp walls. The well-defined donut patterns were observed only when the film thickness was thicker than 50 nm and thinner than 70 nm. We found that the films thinner than 30 nm normally generated dual-line patterns and the second stamping created isolated rectangular small dots, as demonstrated in Figure 8B for the 20-nm-thick film. From the AFM height profile, the rectangular dot patterns had a width of 600 nm, a length of 900 nm, and a height of 90 nm. Based on the figure, the liquid clearly was bound to the PDMS side and remained dewetted on the substrate. A close look at Figure 8B reveals small polymer droplets in the second stamping direction. The small droplets were generated during the translocation of the polymer chains to the PDMS walls. The polymer liquid lines retracted during the second stamping, and some of the chains remained

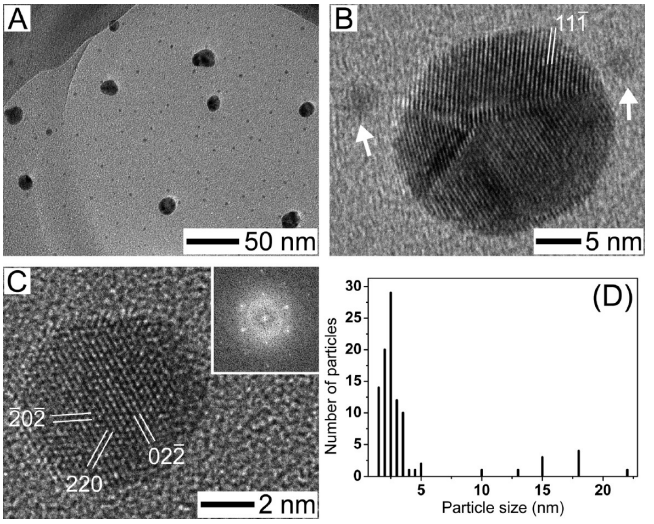

Figure 11. TEM images of Au nanoparticles obtained after reducing the Au precursors with N_2H_4 vapor in the PEO/$HAuCl_4$ composite films: (A) the size of the particles shows a bimodal distribution; (B) HR-TEM image magnifying the particles shown in panel A (small nanoparticles (< 3 nm) are indicated with white arrows); (C) enlarged image of the small nanoparticles, showing their single crystalinity; and (D) size distribution of the nanoparticles, which shows a biomodal distribution.

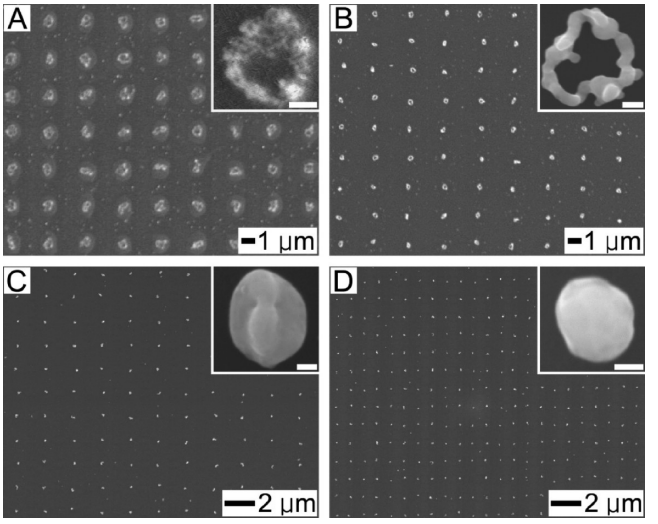

Figure 12. SEM images of Au nanoparticles obtained from the PEO/$HAuCl_4$ composite patterns: (A) backscattering mode image taken after reducing $HAuCl_4$ with N_2H_4 vapor (the enlarged image in the inset shows Au nanoparticles located at the edge of each dot pattern); (B) Au rings obtained after thermal sintering at 350 °C (the inset image presents a continuous Au ring pattern); (C) Au dots obtained after sintering the samples in Figure 9A; and (D) Au dots obtained after sintering the samples in Figure 9B. The insets show enlargements of the sintered Au dots. The scale bars in the insets in panels A and B are 200 nm, and those in panels C and D are 50 nm.

during the migration of the polymer chains to form the small polymeric debris.

The undesired small debris could be removed by taking advantage of the Ostwald ripening process. The results in Figure 9 were obtained from the single-line and dual-line patterns. The specimens were first flipped over and annealed at 130 °C for 10 min. From AFM analysis, the single-dot patterns had a width of 1.8 μm, a length of 1.1 μm, and a height of 170−180 nm and the dual dot patterns had a width of 600 nm, a length of 900 nm, and a height of 80−90 nm. Both figures indicate that most small droplets were absorbed by the larger regular dots. The dots became somewhat rounded during the ripening process to minimize their surface energy, although their overall shape remained the same, regardless of the annealing time. Note that the coupled dots merged with each other when they were annealed at temperatures of > 150 °C.

The second stamping was exerted at different angles to generate various shapes of composite patterns. Figure 10 exhibits the composite patterns at 60°, with respect to the composite lines obtained after the first stamping. Figures 10A and 10B were obtained with single-lined and dual-lined patterns. We found the composite pattern followed the interface with the PDMS stamp to form large or small diamond-like patterns. As seen in the height profiles in Figures 10C and 10D, we could not observe residual layers, except small polymeric debris.

The periodic patterns of the polymer/Au precursor composite can be utilized to generate regularly arrayed Au particles. Simple chemical reduction of the Au precursors produced Au nanoparticles. Figure 11 demonstrates the Au nanoparticles chemically reduced from the composite with the precursor ratio of $\alpha = 0.086$. The specimen was placed in a closed conical tube containing a few drops of hydrazine hydrate. The hydrazine vapor successfully reduced the Au precursor without damaging the PEO chains.

$$4H^+(aq) + 4AuCl_4^-(aq) + 3N_2H_4(g) \rightarrow 4Au(s) + 16HCl(g) + 3N_2(g)$$

Complete reduction took < 5 min. As seen in the TEM image of Figure 11A, the size of the particles were largely discriminated into ~10-nm-level nanoparticles and ~2-nm-level nanoparticles. We found that many of the relatively larger particles (~10 nm) had a twinned structure, as shown in Figure 11B. The small nanoparticles (less than ~3 nm) were single crystalline, as seen in an enlargement in the high-resolution transmission electron microscopy (HR-TEM) image shown in Figure 11C. Some particles even larger than 20 nm were observed to be composed of multiple grains. The size of the Au nanoparticles exhibits a bimodal distribution, as displayed in Figure 11D. The formation of the two different state of particles is not well-understood at the current stage and left for the future study.

The shape of the Au particles might be controlled by adding some capping agents or polymers with amines or acids groups, as well as adjusting the reduction rate. The process discussed in this study may be applicable to any precursors that can form atomic coordination with polymers once the following conditions are met:

(i) Macroscopic phase separation between the metal precursors and the polymers must be restricted;

(ii) Good chain mobility of the crystalline polymers is a benefit to prevent the remnant layer after CFL process; and

(iii) The interfacial energy should change as the precursor concentration varies. In this study, the coordinated

PEO chains increased the interfacial energy with the oxide surface of the Si wafer.

Figure 12A demonstrates the sample shown in Figure 6C after the Au precursors have been reduced by N_2H_4 vapor. The image was taken in the backscattering mode of SEM analysis to track the position of the reduced Au particles in the polymer dots. The inset image clearly verifies that the Au nanoparticles were phase-separated from the PEO polymer matrix and located at the edge of each dot pattern. Since the precursors are coordinated with ethers in PEO backbone chains, they are considered to be uniformly distributed in each pattern. The migration of the Au nanoparticles to the droplet edge is attributed to the reduced strength of the complexation between the Au nanoparticles and PEO chains. Once the binding force is weakened, the hydrophobic Au nanoparticles can move to the edge of the PEO dots and play as a surfactant to reduce the interfacial tension between the substrate and the PEO dots.[21] The as-reduced Au nanoparticles could be merged into one large irregular nanoring by thermally annealing at 350 °C. Figure 12B shows the result of thermal treatment on the same sample shown in Figure 12A. The reduced melting temperature of the Au nanoparticles enabled the consolidation between them at the temperature. Instead of rings, solid Au dots could be obtained by concentrating the as-reduced nanoparticles to the center of each polymer dot. The specimens were flipped over and annealed at 130 °C for 10 min, and then they were thermally annealed at 350 °C. Since the autoignition temperature of PEO is 305 °C in air, the condition in this study (350 °C with oxygen purging, 3 h) is sufficient for complete burnout. We could not observe any organic traces in the SEM and EDX analysis. During the first annealing, the heavy Au nanoparticles were concentrated at the central tip of the flipped polymer droplet and sintered into one solid Au nanoparticle at the central position of each polymer dot. Small droplets disappeared during the sintering by the Ostwald ripening. The FE-SEM images in Figures 12C and 12D demonstrate the solid Au particles obtained from the sample in Figures 7A and 7B, respectively.

(21) Sohn, B.-H.; Choi, J.-M.; Yoo, S., II; Yun, S.-H.; Zin, W.-C.; Jung, J. C.; Kanehara, M.; Hirata, T.; Teranishi, T. *J. Am. Chem. Soc.* **2003**, *125*, 6368.

Conclusions

We have demonstrated that the surface energy of the polymer/organometallic precursor composite films can change by a significant extent as the fractional composition of the precursor increases. In turn, the large change of the surface energy may lead to different patterns by capillary force lithography (CFL) from those of the pure polymer or composites with small amount of precursors. We performed a model study with poly(ethylene oxide) (PEO) and the gold precursor ($HAuCl_4$). When the atomic ratio of the precursor to the ethylene oxide unit (α) over a critical value ($\alpha = 0.086$), the composite liquids remained dewetted on the hydrophilic silicon wafer while their compatibility to the poly(dimethylsiloxane) (PDMS) stamp wall was enhanced. The reduced wettability on the substrate resulted in isolated dot patterns by simply cross-stamping a second stamp on the line patterns. The size and number of the dots could be controlled by adjusting the thickness of the composite films, producing small coupled dots from dual-line patterns and large single dots from single-line patterns. We also exhibited that chemical reduction of the precursors could generate periodic arrays of Au rings or solid nanodots. Because the technique described here can be easily extended to the large-area patterning of nanometer-scale features, it has good potential for the high throughput of periodic arrays of inorganic nanomaterials.

Acknowledgment. We would like to acknowledge the financial support from the Pioneer Research Program of KOSEF (008-05103) and the World Class University Program (R32-20031) by the National Research Foundation (NRF). Y.S.K acknowledges the support from MEST (No. 2009-0079463 and No. R15-2003-032).

Supporting Information Available: AFM images used for contact angle measurement and height profiles for the dots and rings of PEO/Au precursor composites. (PDF) The information is available free of charge via the Internet at http://pubs.acs.org.